Journal of Alloys and Compounds 625 (2015) 52–56

Contents lists available at ScienceDirect

Journal of Alloys and Compounds

journal homepage: www.elsevier.com/locate/jalcom

Using nanoindentation and cathodoluminescence to investigate the residual stress of ZnSe

Hua-Chiang Wen [a,*], Wu-Ching Chou [a,*], Wei-Hung Yau [b], Wen-Chung Fan [a], Ling Lee [c], Kun-Feng Jian [a]

[a] Department of Electrophysics, National Chiao Tung University, Hsinchu 300, Taiwan, ROC
[b] Department of Mechanical Engineering, Chin-Yi University of Technology, Taichung 400, Taiwan, ROC
[c] Center of Nanoscience and Technology, Tunghai University, Taichung 400, Taiwan, ROC

ARTICLE INFO

Article history:
Received 17 February 2014
Received in revised form 28 October 2014
Accepted 28 October 2014
Available online 26 November 2014

Keywords:
ZnSe
Nanoindentation
Cathodoluminescence
Transmission electron microscopy

ABSTRACT

In this study we examined the effects of the nanoindentation-induced residual stress of single-crystalline zinc selenide (ZnSe). We employed the nanoindentation technique to evaluate the dislocation mobility of ZnSe at loading ratios of 10 and 2 mN/min, with a holding time of 120 s under a constant load. We visualized the resultant dislocation and microcracks using cathodoluminescence (CL) spectroscopy and mapping to compare the nanoindentation-induced residual stresses of the various ZnSe samples. CL mapping revealed massive dislocation activities during the loading process. The dislocations played roles as nonradiative recombination centers that quenched the local CL intensity. Transmission electron microscopy also revealed the effects of nanoindentation-induced residual stress. To obtain insight into the influence of the residual stress and to determine the dislocation mobilities for ZnSe films, it was essential to monitor the quenching effect of nonradiative recombination centers as a function of CL mapping.

© 2014 Elsevier B.V. All rights reserved.

1. Introduction

ZnSe has great potential for application in photonic devices. For example, high-performance photodetectors of ultraviolet light have been demonstrated using p-type ZnSe:Sb nanowires [1]; compact mid-infrared channel waveguide lasers have been fabricated using Cr-doped ZnSe [2]; and ZnSe scintillation crystals of high quantum yield have been used to manufacture X-ray detectors [3,4]. The performance of such thin films remains limited, however, because of defect generation and propagation [5–7]. Nanoindentation is an effective technique for studying mechanical properties under contact loading [8], as well as for investigations of nanotribology [9,10]. This technique has been used very successfully to measure the hardnesses and Young's moduli of ZnCdSe [11], ZnMnO [12], and GaN [5,13]; it has also been employed to measure the hardness response of ZnSe *in situ* [14,15]. When Jian and Lee [16] studied the nanoindentation-induced pop-in effects in ZnSe thin films, they found that the critical loading and estimated dislocation loops were due to homogeneous nucleation of dislocations; nevertheless, the effects of residual stress during nanoindentation tests remained unclear. They could not determine the indenter-induced *in situ* mobility of dislocation; only, indirectly, the displacement response during the unloading of the nanoindentation curve. Recently, we employed cathodoluminescence (CL) to reveal the dynamics of recombination-enhanced dislocation of ZnSe materials under nanoindentation [17]. We found that the indenter could be sensitive to the prevailing stress conditions, where the obtained load–penetration depth curve acted as a fingerprint of the material under study. Jian and Lin [18] reported the mechanical responses of single-crystal ZnO in conjunction with CL images, revealing a rosette structure for ZnO with hexagonal symmetry. Lee and Kwon [19] reported indentation depth–controlled stress relaxation combined with a shear plastic-deformation. In addition, Lee et al. [20] used CL to study GaAs nanowires as a function of the trench width. CL has also revealed the effective trapping of the threading dislocation and the stacking fault in the Si(001) trench of semi-polar GaN [21]. Thus, CL has been a very powerful tool for studying the defect generation and propagation in various samples after indentation.

In this study we investigated the nanoindentation-induced residual stress in ZnSe, employing CL to examine the Berkovich-induced deformation of ZnSe and the quasistatic technique to measure its time-dependent plasticity. CL image mapping can be used to identify the differences in residual stress induced by various loading rates. Accordingly, we employed this approach to develop a method for measuring residual stresses in brittle materials using cube-corner indentation as the probing indent.

* Corresponding authors. Tel.: +886 (3) 5712121x56129; fax: +886 (3) 5725230.
E-mail addresses: a091316104@gmail.com (H.-C. Wen), wuchingchou@mail.nctu.edu.tw (W.-C. Chou).

http://dx.doi.org/10.1016/j.jallcom.2014.10.162
0925-8388/© 2014 Elsevier B.V. All rights reserved.

2. Experimental details

The (100)-oriented ZnSe substrates were cut from crystals grown through solid phase recrystallization. The detailed growth procedures to prepare ZnSe single crystals have been described previously [22]. To investigate the mechanical properties, nanoindentation measurements were performed using a Nanoindenter MTS NanoXP system (MTS, Nano Instruments Innovation Center, TN, USA) equipped with a diamond pyramid-shaped Berkovich-type indenter tip (radius of curvature: 50 nm). Stiffness data were recorded along with load and displacement (*P*–*d*) curves. The hardness and Young's modulus of ZnSe were calculated using the analytical method developed by Oliver and Pharr [23,24]; each value, reported here with its standard deviation, was averaged from 10 indentations. The thermal drift was maintained below ±0.05 nm/s for all indentations considered.

A 10 × 1 indentation array was created, with each indentation separated by 50 μm. Through this method, uncertain interactions and noises between each indentation mark could be avoided. Each indentation was controlled using an indentation load of 100 mN from the loading/unloading *P*–*d* curve. In each indentation test, the Berkovich diamond indenter was operated with typical nanoindentation *P*–*d* curves at a loading ratio (LR) of either 10 or 2 mN/min and a holding time (HT) of 120 s.

The effect of nanoindentation-induced mechanical deformation on the optical properties of ZnSe were characterized at 300 K through CL spectroscopy and monochromatic mapping, determined using scanning electron microscopy (SEM; JEOL JSM-7001F, operated at 16 keV and 15 nA). The spot size of the electron beam was less than 10 nm under these conditions. The CL signals were analyzed using a Horiba Jobin–Yvon iHR550 0.5 m monochromator and detected by a liquid N_2-cooled charge coupled device (CCD) with an energy resolution of 0.3 meV [17]. The morphologies and microstructures were also examined using SEM and transmission electron microscopy (TEM; JEOL-JEM 2100F operated at 200 kV; point-to-point resolution: 0.23 nm; lattice resolution: 0.14 nm).

3. Results and discussion

Fig. 1 presents load–displacement (*P*–*d*) plots of the ZnSe sample. The maximum applied load (P_{max}) was 100 mN. The curves were recorded at loading ratio (LR) of 10 and 2 mN/min. The displacement curves of loading and unloading feature three steps: (i) initial loading, (ii) holding time (HT, 120 s), and (iii) unloading. The two curves illustrate the residual stress in terms of the apparent separation when the penetration was 700 nm. Compared with curve (a), we observed a lower plastic work of indentation (W_p) for curve (b). The existence of residual stress is due to the formation of pile-up [25,26]. The penetration depths, $d_{LR=10}$ and $d_{LR=2}$, at the end of the initial loading period were 1609 and 1672 nm, respectively, when the LRs were 10 and 2 mN/min, respectively. The value of the error in depth (d_{err}), given by $(d_{LR=2}–d_{LR=10})/d_{LR=2}$ was 3.78%. As listed in Table 1, the measured hardness and modulus at an LR of 10 mN (2 mN) were 1.34 ± 0.04 (1.33 ± 0.03 GPa) and 79.2 ± 1.2 (79.7 ± 1.5 GPa), respectively. These values of hardness (and modulus) are very similar, suggesting that they were independent of the LR. In a previous investigation [17], we also observed the residual stress phenomenon. In this present study, we found that the unloading process ended earlier when the LR was 2 mN/min, due to the presence of less residual stress than that obtained at 10 mN/min (Fig. 1). Furthermore, we observed cracks (indicated by the arrow) arising from anisotropic cube-corner indenter in the SEM images of the sample treated with an LR of 10 mN/min. In contrast, no clear cracks appeared when the LR was 2 mN/min, due to the lower residual stress; the shadowed area around the intender implies an accumulation of the stress field, presumably due to the high density of the extended defects.

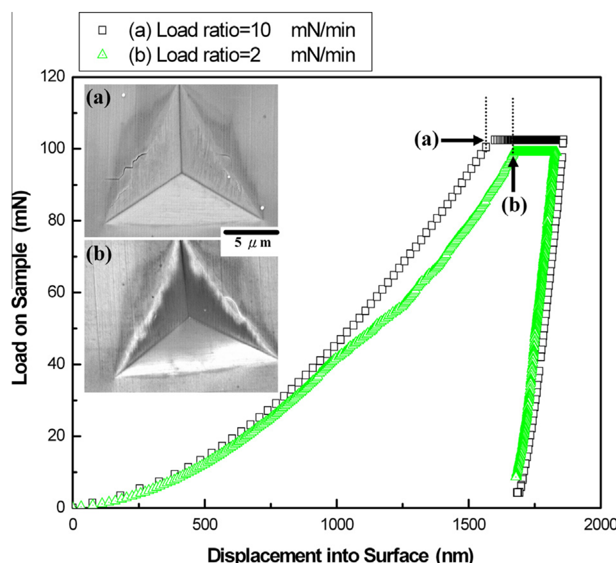

Fig. 1. Load–displacement curves for ZnSe during loading/unloading cycles at loading ratios of (a) 10 and (b) 2 mN/min.

Fig. 2(a) displays the CL spectra recorded at a temperature of 300 K for the samples that had been subjected to an LR of 10 mN/min. The main luminescence peak at 2.68 eV was due to the near band edge emission of ZnSe. We attribute the very broad emission from 1.8 to 2.4 eV to defect emissions. Fig. 2(b) presents the polychromatic CL image. Compared with the non-indented zone (I), clear dislocations of the dark lines were evident in the indented zones (II) and (III). We also investigated the propagation of dislocation, due to plastic deformation, away from the indenter. First, we observed that the cube-corner indenter formation and some extended defects reflected some of the radial symmetry of the stress field. We ten used the CL system to excite the residual indentations. The near-bandgap CL emission was, therefore, suppressed dramatically, owing to those induced defects and/or dislocations. Previous reports have revealed Star of David-like distributions of defects reflected from GaN samples via a spherical indenter, displayed in a symmetrical image [27,28]. Note, when applying a Berkovich-type indenter tip, CL monochromatic imaging can be employed to separate indentations that have undergone LR cycles during plastic deformation.

Fig. 3(a) displays the CL spectrum at a temperature of 300 K for the sample that had been subjected to an LR of 2 mN/min. Fig. 3(b) presents the full-band CL image, revealing the distribution of indentation-induced extended defects that altered the CL emission. When we compare the effects of the typical loading of the indentation center, both the CL emission and CL images revealed that an LR of 2 mN/min (Fig. 3) was more stable than a value of 10 mN/min (Fig. 2). This behavior can be attributed to (i) the amount of residual stress found at an LR of 10 mN/min being larger than at 2 mN/min, when the error depth is given as 3.78%; (ii) the increased amount of elastic recovery almost overlapping at the unloading of the indenter displacement; and (iii) a decrease in the value of d_{max} at the maximum value of P_{max} being expected to decrease the value of W_p (residual stress). A similar investigation revealed previously that the CL intensity measured in the bulk was lower than that of a residual indent [29]. The extent of radial propagation of contact-induced defects in ZnO has also been noted to dramatically suppress the CL near-bandgap emission from the central regions of the residual indent impressions [30]. It has also been suggested that irradiation has an effect on the CL spectra, resulting in complex formation or charge transfer processes induced by new point defects (2.0–2.2 eV) and higher concentrations of point defects in deformed samples [14]. Yau et al. [17] found that dislocations acted as nonradiative recombination centers that quenched the luminescence locally. In this present study, we estimated both the CL spectrum and mapping of the indented area of the ZnSe sample. Although we did not observe a critical "pop-in" phenomenon, we did find a distinct decrease in the near-bandgap emission and a relative decay in the intensity of the broad emission.

Table 1
Measured hardnesses and moduli.

No.	Loading ratio (N/min)	Holding time (s)	Modulus (GPa)	Hardness (GPa)
1	10	120	79.2	1.34
2	2	120	79.7	1.33

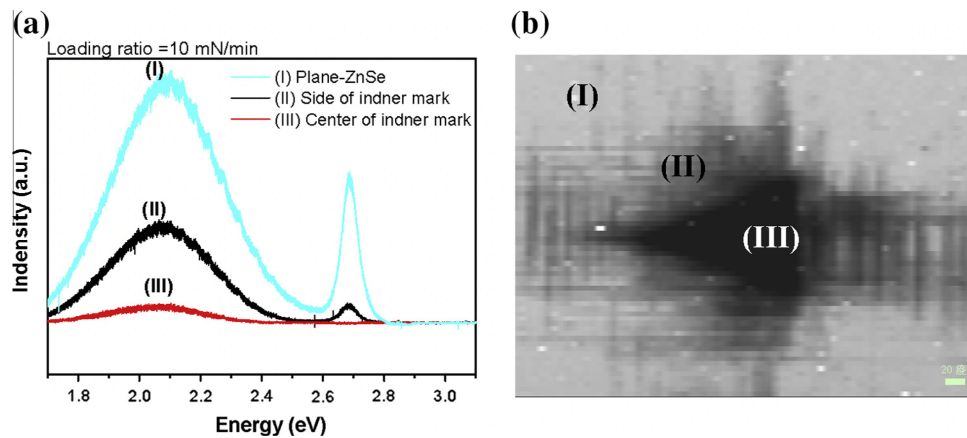

Fig. 2. (a) CL spectra and (b) CL mapping of ZnSe samples at liquid N_2 temperature, after being subjected to an LR of 10 mN/min, measured at various capture areas: (I) plane-ZnSe; (II) side of indenter mark; (III) center of indenter mark.

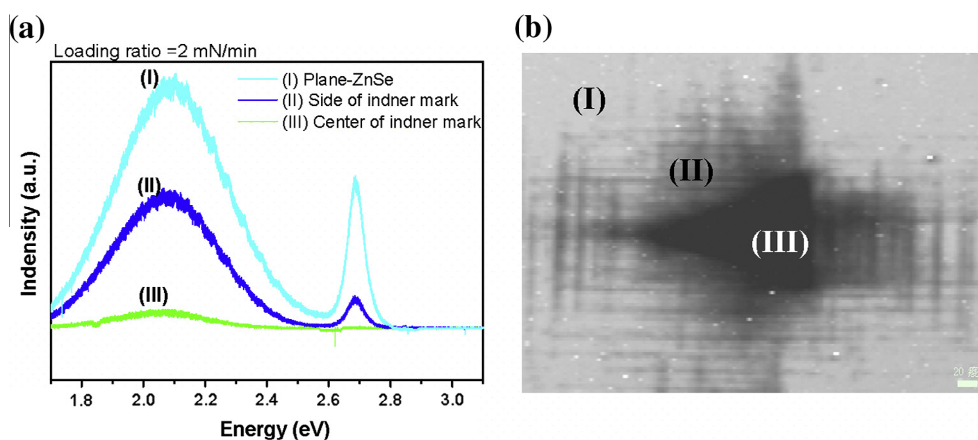

Fig. 3. (a) CL spectra and (b) CL mapping of ZnSe samples at liquid N_2 temperature, after being subjected to an LR of 2 mN/min, measured at various capture areas: (I) plane-ZnSe; (II) side of indenter mark; (III) center of indenter mark.

We used TEM to characterize the compressed indenter marks on the ZnSe surfaces. The TEM surface profile in Fig. 4(a) reveals significant cube-corner indentation; we could not, however, observe extended defects of the stress field. In the ZnSe bulk, the residual indent area was evident with a clean image. Top-view selected area diffraction pattern (SADP) analysis (Fig. 4(b)) revealed the ZnSe bulk behavior of the spot. We employed SADP also to identify extended defects of the stress field of the ZnSe (Fig. 4(c)). The pattern clearly reveals the presence of different mixture phases that we attribute to possible massive dislocation slip traces within the side of the indentation zone, consistent with our CL observations. In Fig. 4(d), the distributions of the corresponding phases are highlighted as bright areas within the center of the indentation zone; the polycrystalline phase dominates the center of the indent. The SADPs revealed a clear halo ring pattern at the center of the indentation zone, with some amorphous or mesocrystalline regions found through TEM analyses. We suggest that some dislocations tend to follow the directions of easy slip and may be pinned between slip bands [31]. Yau et al. [17] noted that slip bands and dislocations could slip partially along easy-slip directions. The molecular bonds of indented ZnSe are influenced by dislocation propagation. Fig. 4(d) displays the specific microstructure of a heavily deformed material, confirmed by features having a high density of dislocations. These results are consistent with our CL mapping, nanoindentation, and SEM observations. In the case of artificial nanoindentation, high dislocation densities indicate a highly strained state of ZnSe with distorted slip bands. Previous studies have demonstrated that the primary slip system of the ZnSe sphalerite structure is $(1\,1\,1)\,\langle 1\,-1\,0\rangle$, consisting of five independent systems; with strong asymmetry between the dislocation mobilities of the Zn- and Se-terminated dislocations in the active glide-set, the mobility of the Se(g) dislocations is 100 times higher than that of the Zn(g) dislocations [32–36]. Yau et al. [17] suggested that the primary slip system of ZnSe may play an important role during nanoindentation, where the CL spectrum displays the enhancement of a very broad CL emission (2.1 eV), greater than that of typical indentation loading. It has been reported previously that the total CL intensity of the deformed samples can be

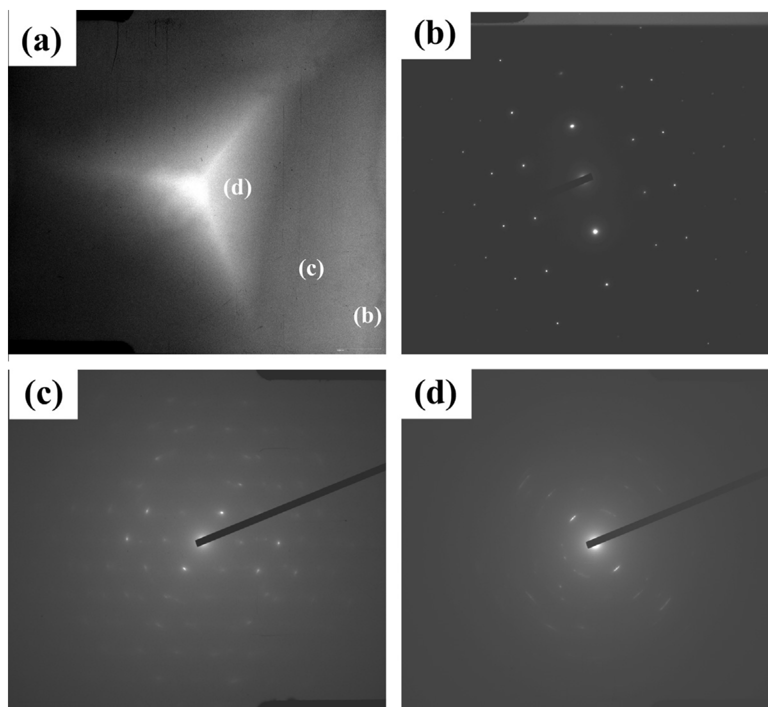

Fig. 4. (a) Cross-sectional TEM images of a ZnSe sample subjected to typical loading/unloading cycles (plan view). (b–d) SADP analyses of (b) the non-indented ZnSe bulk material (the spot was clearly observable on the top view); (c) the extended defects of the stress field of the ZnSe; (d) a specific microstructure of a heavily deformed material, confirmed by features having a polycrystalline phase dominating the center of the indentation.

decreased as a result of the amount of dark lines from the slip bands [16]. In addition, the excitonic emissions of ZnO samples are quenched at the indent site [26,32]. In this present study, we observed changes in the CL spectra and the dark slip lines of ZnSe, revealing a quenching of the luminescence in the indentation mark; the area displays dark lines corresponding to slip bands (Figs. 2 and 3). Concerning the cube-corner indenter, CL mapping suggested that the main extended lines were nonradiative defect bands, with those defects extending away by means of the indent site or by strain-induced migration away from the defect bands. After varying the LR cycles, in which a partial percentage of indentations were under elastic recovery, CL imaging could directly separate the effects of both types of LR indentations. An observable CL impression, therefore, provided convincing evidence that the result involved the nucleation of a slip while deformation occurred (Fig. 1). In closing, the main deformation mechanisms for ZnSe are dislocation nucleation and propagation, depending on the easy-slip systems [17]. The mechanism in the elastic recovery of ZnSe appears to be associated with the activation of dislocation sources through both LR cycles of indentation. The residual stress plays the dominant role when artificial nanoindentation occurs.

4. Conclusions

Employing a combination of nanoindentation, CL, SEM, and TEM techniques, we have investigated the elastic recovery of ZnSe by examining its contact-induced structural deformation behavior. From our CL analyses, we estimate, for the strains, that the amount of residual stress that can be found when the LR was 10 mN/min is larger than that found at 2 mN/min, when the error depth is 3.78%. The indenter areas acted as a non-radiative recombination center, with CL mapping suggesting that the main extended lines might be a signal of nonradiative defect bands. Plane-view SEM/TEM images revealed that the prime deformation mechanism in ZnSe was slip nucleation on both the basal and pyramidal planes. SADP characterization of the ZnSe samples clearly revealed a halo ring pattern at the non-indented area, with distortion of the ring pattern at the center of the indentation area and an amorphous or mesocrystalline region. This approach allows investigations of nanoindentation-induced residual stress on ZnSe; it confirms that CL is a powerful tool for studying defect generation and propagation of samples after indentation.

Acknowledgments

This research was supported by the National Science Council in Taiwan under Contract (102-2119-M-002 -004 and MOST 103-2119-M-009 -002). The author thanks Professor Wu-Ching Chou for assistance with the CL measurements (JEOL JSM-7001F field-emission scanning electron microscope) and helpful discussions.

References

[1] B. Nie, L.B. Luo, J.J. Chen, J.G. Hu, C.Y. Wu, L. Wang, Y.Q. Yu, Z.F. Zhu, J.S. Jie, Nanotechnology 24 (2013) 095603 (8pp).
[2] J.R. Macdonald, S.J. Beecher, P.A. Berry, K.L. Schepler, A.K. Kar, Appl. Phys. Lett. 102 (2013) 161110.
[3] J.R. Macdonald, S.J. Beecher, P.A. Berry, G. Brown, K.L. Schepler, A.K. Kar, Opt. Lett. 38 (2013) 2194–2196.
[4] V.A. Litichevskyi, A.D. Opolonin, S.N. Galkin, A.I. Lalaiants, E.F. Voronkin, Instrum. Exp. Tech. 56 (2013) 436–443.
[5] P.F. Yang, S.R. Jian, Y.S. Lai, C.S. Yang, R.S. Chen, J. Alloys Comp. 463 (2008) 533–538.
[6] S.R. Jian, J.S.C. Jang, G.J. Chen, H.G. Chen, Y.T. Chen, J. Alloys Comp. 479 (2009) 348–351.
[7] S.R. Jian, Y.-H. Lee, J. Alloys Comp. 587 (2014) 313–317.
[8] S.R. Jian, J.S.C. Jang, J. Alloys Comp. 482 (2009) 498–501.
[9] M.H. Lin, H.C. Wen, Y.R. Jeng, C.P. Chou, Nanoscale Res. Lett. 5 (11) (2010) 1812–1816.
[10] M.H. Lin, H.C. Wen, C.Y. Huang, Y.R. Jeng, W.F. Wu, C.P. Chou, Appl. Surf. Sci. 256 (2010) 3464–3467.
[11] H.C. Wen, C.S. Yang, W.C. Chou, Appl. Surf. Sci. 256 (2010) 2128–2131.
[12] Y.M. Chang, H.C. Wen, C.S. Yang, D. Lian, C.H. Tsai, J.S. Wang, W.F. Wu, C.P. Chou, Microelectron. Reliab. 50 (2010) 1111–1115.
[13] S. Basu, M.W. Barsoum, A.D. Williams, T.D. Moustakas, J. Appl. Phys. 101 (2007) 0835221–0835227.

[14] P. Fernández, J. Piqueras, A. Urbieta, Y.T. Rebane, Y. Shreter, Semicond. Sci. Technol. 14 (1999) 430–434.
[15] S.E. Grillo, M. Ducarroir, M. Nadal, E. Tournié, J.P. Faurie, J. Phys. D Appl. Phys. 35 (2002) 3015–3020.
[16] S.R. Jian, Y.H. Lee, J. Alloys Comp. 494 (2010) 214–218.
[17] W.H. Yau, P.C. Tseng, H.C. Wen, C.H. Tsai, W.C. Chou, Microelectron. Reliab. 51 (2011) 931–935.
[18] S.R. Jian, Y.Y. Lin, J. Alloys Comp. 590 (2014) 153–156.
[19] Y.H. Lee, D. Kwon, Scri. Mater. 49 (2003) 459–465.
[20] L. Lee, K.F. Chien, W.C. Fan, W.C. Chou, C.H. Ko, C.H. Wu, Y.R. Lin, C.T. Wan, C.H. Wann, C.W. Hsu, Y.F. Chen, Y.K. Su, J. Appl. Phys. 51 (2012) 06FG15.
[21] L. Lee, K.F. Chien, W.C. Chou, C.H. Ko, C.H. Wu, Y.R. Lin, C.T. Wan, C.H. Wann, C.W. Hsu, Y.F. Chen, Y.K. Su, Cryst. Eng. Commun. 14 (2012) 4486–4489.
[22] R. Triboulet, J.O. Ndap, A. Tromson-Carli, P. Lemasson, C. Morhain, G. Neu, J. Cryst. Growth 159 (1996) 156–160.
[23] F. Wang, P. Huang, K. Xu, Surf. Coat. Technol. 201 (2007) 5216–5218.
[24] W.C. Oliver, G.M. Pharr, J. Mater. Res. 7 (1992) 1564–1583.
[25] S.J. Bull, J. Phys. D Appl. Phys. 38 (2005) R393–R413.
[26] M.K. Khan, M.E. Fitzpatrick, S.V. Hainsworth, A.D. Evans, L. Edwards, Acta Mater. 59 (2011) 7508–7520.
[27] S.O. Kucheyev, J.E. Bradby, J.S. Williams, C. Jagadish, M. Toth, M.R. Phillips, M.V. Swain, Appl. Phys. Lett. 77 (2000) 3373–3375.
[28] S.O. Kucheyev, J.E. Bradby, J.S. Williams, C. Jagadish, M.V. Swain, G. Li, Appl. Phys. Lett. 78 (2001) 156–158.
[29] V.A. Coleman, J.E. Bradby, C. Jagadish, M.R. Phillips, Appl. Phys. Lett. 89 (2006) 0821021–0821023.
[30] J.E. Bradby, S.O. Kucheyev, J.S. Williams, C. Jagadish, M.V. Swain, P. Munroe, M.R. Phillips, Appl. Phys. Lett. 80 (2002) 4537–4539.
[31] M.H. Zaldívary, P. Fernández, J. Piqueras, Semicond. Sci. Technol. 13 (1998) 900–905.
[32] B. Wolf, A. Belger, D.C. Meyer, P. Paufler, Phys. Status Solidi (a) 187 (2001) 415–426.
[33] M.V. Nazarov, Mater. Sci. Eng. B91–2 (2002) 349–352.
[34] Y.A. Osipyan, V.F. Petrenko, A.V. Zaretskij, R.W. Whitworth, Adv. Phys. 35 (1986) 115–188.
[35] Z. Mierczyk, A. Majchrowski, W. Gruhn, Opt. Lasers Technol., (UK) 35 (2003) 169–172.
[36] M.G. Brik, I.V. Kityk, Phys. Status Solidi (b) 245 (2008) 163–169.